Journal of the Serbian Chemical Society
JSCS-info@shd.org.rs • www.shd.org.rs/JSCS
J. Serb. Chem. Soc. *83* (6) 707–721 (2018)
JSCS–5106
UDC 547.233'821+547.56:519.677:577.213.3+543.422–76:57–188
Original scientific paper

DFT calculation, biological activity, anion sensing studies and crystal structure of (*E*)-4-chloro-2-[(pyridin-2-ylimino)-methyl]phenol

NURAY YILDIRIM[1], NESLİHAN DEMİR[2], GÖKHAN ALPASLAN[3], BAHADIR BOYACIOĞLU[4], MUSTAFA YILDIZ[5]* and HÜSEYİN ÜNVER[6]

[1]Health Services Vocational School, Çanakkale Onsekiz Mart University, TR-17100 Çanakkale, Turkey, [2]Department of Biology, Faculty of Arts and Sciences, Çanakkale Onsekiz Mart University, TR-17100 Çanakkale, Turkey, [3]Department of Medical Services and Techniques, Vocational School of Health Services, Giresun University, TR-28200 Giresun, Turkey, [4]Vocational School of Health Services, Ankara University, TR-06290 Keçioren-Ankara, Turkey, [5]Department of Chemistry, Faculty of Arts and Sciences, Çanakkale Onsekiz Mart University, TR-17100 Çanakkale, Turkey and [6]Department of Physics, Faculty of Science, Ankara University, 06100 Beşevler-Ankara, Turkey

(Received 2 October, revised 28 November, accepted 25 December 2017)

Abstract: (*E*)-4-Chloro-2-[(pyridin-2-ylimino)methyl]phenol was synthesized in the reaction of 2-aminopyridine with 5-chlorosalicylaldehyde. The structure of compound was investigated by FTIR, UV–Vis, ^{1}H-NMR, ^{13}C-NMR and X-ray data. In addition, characterization of the compound was realized using theoretical quantum mechanical calculations and experimental spectroscopic methods. The molecular structure of the compound was confirmed using X-ray single-crystal data, NMR, FTIR and UV–Vis, which were in good agreement with the structure predicted by the theoretical calculations using the density functional theory (DFT). Moreover, the antimicrobial activity of the compound was investigated against some bacteria and yeast cultures by the broth micro-dilution test. UV–Vis spectroscopy studies of the interactions between the Schiff base and calf thymus DNA (CT-DNA) showed that the compound interacts with CT-DNA *via* electrostatic binding. The colorimetric response of the compound receptors was investigated before and after the addition of an equivalent amount of each anion to evaluate anion recognition properties.

Keywords: UV–Vis spectroscopy; 2-aminopyridine; anti-microbial activity; DNA binding; X-ray crystallography.

INTRODUCTION

Schiff bases and their metal complexes have attracted curiosity due to their DNA binding and cleavage properties.[1–5] Applications of them as chemical nuc-

* Corresponding author. E-mail: myildiz@comu.edu.tr
https://doi.org/10.2298/JSC171001009Y

Available on line at www.shd.org.rs/JSCS/
(CC) 2018 SCS.

leases is the focus of current research. It has been demonstrated that they could be used in some studies as sequence specific DNA binding agents, and diagnostic agents in medicinal applications and for genomic research.[6–9] They were used as ligands and their complexes were used in a wide range of medicinal chemistry.[10–12]

The tautomeric balance and intramolecular hydrogen bond in Schiff bases occur through proton transfer, leading the compound to exhibit interesting physical and biological properties that have attracted the attention of researchers. Studies on the physical and chemical properties of Schiff bases in solid state and in solution continue. Molecules creating intramolecular bonds[13] are used in highly specific systems because of their high thermodynamic stability.[14]

Schiff bases are important to synthesize sensors for recognizing and sensing anions, and to enlarge their areas of use. The intramolecular hydrogen bond and proton transfer explained above are thought to affect anion-sensory properties.[15–17] It could be specifically stated that the keto-amine and enol-imine tautomer balances contribute to the bonding and selection of anions. Undoubtedly, colorimetric anion sensors are of more importance, because such materials are useful as they provide visual information more readily. Various studies have been performed in order to develop these materials.[18,19]

In the present work, the Schiff base (*E*)-4-chloro-2-[(pyridin-2-ylimino)-methyl]phenol (Fig. S-1, of the Supplementary material to this paper) was prepared and studied by experimental (UV–Vis, FTIR, NMR and X-ray diffraction) and computational (density functional theory (DFT)) methods. The molecular structure, HOMO–LUMO analysis, molecular electrostatic potential (*MEP*) and nonlinear optical (NLO) effects of the compound were investigated using DFT calculations. Additionally, the Schiff base was tested for its potential sensor ability to sense anions selectively and for its interaction with DNA.

EXPERIMENTAL

Materials and methods

The ^{1}H- and ^{13}C-NMR spectra were recorded on a Bruker Avance-500 spectrometer operating at 400 and 101.6 MHz, respectively. The infrared absorption spectra were obtained in KBr discs using a Perkin Elmer BX II spectrometer and are reported in cm^{-1} units. The UV–Vis spectra were measured using a Shimadzu 1800 series spectrometer. Elementary analyses were performed on a Vario EL III CHNS elemental analyzer. The melting points were measured with an Electro Thermal IA 9100 apparatus using a capillary tube. 2-Aminopyridine, 5-chlorosalicylaldehyde, DMSO, EtOH, $CHCl_3$, *n*-hexane, $(Bu)_4NF$, $(Bu)_4NBr$, $(Bu)_4NI$, $(Bu)_4NCN$, $(Bu)_4NSCN$, $(Bu)_4NClO_4$, $(Bu)_4NHSO_4$, $(Bu)_4NCH_3COO$, $(Bu)_4NH_2PO_4$, $(Bu)_4NN_3$, $(Bu)_4NOH$ and DMSO were purchased from Aldrich.

Analytical and spectral data are given in the Supplementary material.

*Synthesis of (*E*)-4-chloro-2-[(pyridin-2-ylimino)methyl]phenol*

2-Aminopyridine (0.50 g, 5.32 mmol) was added to an EtOH (100 mL) solution of 5-chlorosalicylaldehyde (0.829 g, 5.32 mmol). The mixture was stirred and refluxed for 1 h.

(CC) 2018 SCS.

The product was obtained by evaporation of the EtOH. It was crystallized from $CHCl_3$:*n*-hexane (3:2 volume ratio) as orange crystals.

X-Ray crystallography

A suitable single crystal of the title compound was mounted on a goniometer and the data were collected at 293 K on a Bruker Kappa APEXII CCD diffractometer using graphite monochromated MoK_α radiation (λ = 0.71073 Å). The cell parameters of the compound were determined using SAINT software.[20] Absorption correction (μ = 0.34 mm^{-1}) was obtained by the multi-scan method *via* SADAPS V2012/1 software.[21] The compound is solved by direct methods using SHELXS-97[22] and refined with SHELXL-97.[22] The molecular figures were prepared with the help of Mercury and ORTEP-3 program packages.[23,24] Details of the data collection conditions and the parameters of the refinement process are given in Table I.

TABLE I. Crystallographic data and structure refinement for the title compound

Chemical formula	$C_{12}H_9ClN_2O$
Crystal shape/color	Prism/orange
Formula weight	232.66
Crystal system	Monoclinic
Space group	$P2_1/n$
Unit cell parameters	
a / 10^{-10} m	4.5628 (4)
b / 10^{-10} m	19.3486 (17)
c / 10^{-10} m	12.0485 (11)
Volume (m^3)	1059.19 (16)
Z	4
D_x / mg cm^{-3}	1.459
μ / mm^{-1}	0.34
F_{000}	480
Crystal size, mm^3	0.18×0.12×0.10
Diffractometer/measurement method	Bruker APEX-II CCD/w and φ scans
Absorption correction	Multi-scan
T_{min}	0.643
T_{max}	0.745
No. of measured, independent and observed reflections	22333, 2177, 1715
Observed criterion	$I > 2\sigma(I)$
R_{int}	0.052
θ_{max}	26.4
Refinement on	F^2
$R[F^2 > 2\sigma(F^2)]$, S	0.060, 1.03
No. of reflections	2177
No. of parameters	150
$\Delta\rho_{max}$, $\Delta\rho_{min}$ / e $Å^{-3}$	0.65, –0.60

Computational procedures

All theoretical computations were realized using Gauss-View5[25] molecular visualization and the Gaussian 09W program package.[26] For the calculation of the molecule geometry, the atomic coordinates obtained from the X-ray geometry were used. The geometry optimization of the title molecule was performed using the DFT method with the Becke three parameters

(CC) 2018 SCS.

hybrid exchange-correlation functional (B3LYP)[27] at the 6-311++G(d,p) basis set.[28] To investigate the reactive sites and to identify sites of intra and intermolecular interactions of the compound, the molecular electrostatic potential surface was evaluated using the B3LYP/6--311++G(d,p) method. The HOMO–1, HOMO, LUMO and LUMO+1 energy values and their shapes were calculated and simulated using the same basis set. The linear polarizability and first hyperpolarizability properties of the compound were obtained from the molecular polarizabilities based on theoretical calculations.

Screening for antimicrobial activities

Bacillus subtilis ATCC 6633, *Staphylococcus aureus* ATCC 25923, *Escherichia coli* ATCC 25922, *Enterococcus faecalis* ATCC 29212, *Pseudomonas aeruginosa* ATCC 27853, *Escherichia coli* ATCC 35218, *Bacillus cereus* NRRL B-3711, *Proteus hauseri* ATCC 13315, *Candida albicans* ATCC 60193 and *Candida tropicalis* ATCC 13803 were used as the test microorganisms. The *MIC* tests were performed by the broth microdilution method in triplicate as outlined in the CLSI guidelines.[29] The inocula were adjusted to a turbidity of 0.5 McFarland standard and diluted to a final concentration from 4×10^5 to 8×10^5 CFU mL^{-1}. The compound was dissolved in DMSO (dimethyl sulfoxide) and serially diluted in cation-adjusted Mueller–Hinton broth for the bacteria or RPMI medium for the yeasts in 96 well plates to a final volume of 100 µL in each well. Then, an equal volume of inocula was added to each well. The concentration of the compound, including control antibiotics ampicillin and antifungal fluconazole ranged between 0.5–256 µg mL^{-1}. The plates were incubated at 37 °C and the results were evaluated after 16–20 h for the bacteria and 24±2 h for the fungi and the *MIC* values were recorded.

DNA-binding experiments

The UV–Vis spectra titrations were performed in Tris–HCl/NaCl buffer at room temperature to investigate the binding affinity between CT-DNA and the Schiff base. The UV–Vis absorbance at 260 and 280 nm of the CT-DNA solution in Tris buffer give a ratio of 1.8–1.9, indicating that the DNA was sufficiently free of protein.[30] Tris–HCl/NaCl buffer (3 mL) and the solutions of Schiff base of buffered CT-DNA solution were added to each cuvette in order to eliminate the absorbance of DNA itself. Before the absorption spectra were recorded, the Schiff base–DNA solutions were incubated at room temperature for 5 min.

Anion sensors measurements

Schiff base (0.006 mmol) was dissolved in DMSO (50 mL). Tetrabutylammonium salts (F^-, Br^-, I^-, CN^-, SCN^-, ClO_4^-, HSO_4^-, CH_3COO^-, $H_2PO_4^-$, N_3^- and OH^-, 0.006 mmol) were dissolved in DMSO (50 mL). Each solution of a tetrabutylammonium salt was added to the Schiff base solution (1:1) in the tube. After mixing, the UV absorption spectra and a photograph were taken at room temperature.

RESULTS AND DISCUSSION

Description of the crystal structure

The title compound crystallizes in the monoclinic space group $P2_1/n$ with $Z = 4$ in the unit cell. The asymmetric unit in the crystal structure contains only one molecule. It is known that tautomeric forms of Schiff base compounds have two types of intramolecular hydrogen bonds, which belong to O–H···N in phenol-imine form and N–H···O in the keto-amine form. The single-crystal

(CC) 2018 SCS.

X-ray study showed that the title compound adopts the phenol-imine tautomeric form. The C7–N1 and C2–O1 bond lengths have a significant influence in determining the tautomeric form. The C7–N1 bond distance (1.278(3) Å) is consistent with a C=N double bond and the C2–O1 bond (1.353(3) Å) is consistent with a C–O single bond. These bond distances are comparable with those of compounds previously reported as phenol-imine.[31–33] The dihedral angle between the C1–C6 and pyridine rings (C8–N2) is 4.38(8)°. The molecular structure is stabilized by an intra-molecular O1–H1···N1 hydrogen bond (Fig. 1). In the crystal structure, molecules are linked to each other by an intermolecular C–H···O hydrogen bond. Atom C7 in the reference molecule at (*x*, *y*, *z*) acts as a hydrogen-bond donor, *via* H7, to atom O1 in the molecule at (*x*–1/2, –*y*+3/2, *z*–1/2), so forming a C(5) chain running parallel to the [001] direction (Fig. S-6 of the Supplementary material). Details of the hydrogen bonds are summarized in Table II.

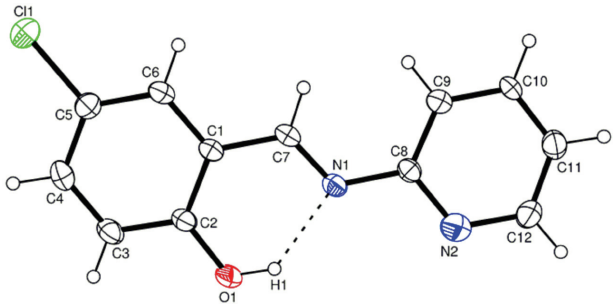

Fig. 1. Ortep-3 diagram of the title compound. Displacement ellipsoids are drawn at the 30 % probability level. The intramolecular hydrogen bond is shown as a dashed line.

TABLE II. Hydrogen-bond geometry (Å, °); symmetry code, *i*: *x*–1/2, –*y*+3/2, *z*–1/2

D–H···A	D–H	H···A	D···A	D–H···A
O1–H1···N1	0.88(5)	1.92(5)	2.622(3)	135(4)
C7–H7···O1^{i}	0.93	2.61	3.487(3)	158

Optimized structure

Geometric optimization of the investigated compound was performed using the DFT/B3LYP method with the 6-311++G(d,p) basis set (Fig. S-7 of the Supplementary material). Some of the bond lengths, bond angles and torsion angles of the optimized structure are listed in Table III and compared with the experimental data of the compound. As can be seen from Table III, most of the molecular geometric parameters are slightly different from the experimental ones. The biggest differences between experimental and calculated bond lengths and angles are 0.058 Å for the C10–C11 bond and 5.3° for the C10–C9–C8 angle, respectively. According to crystallographic studies, the dihedral angle between the C1–C6 and pyridine rings is 4.38(8)°, while this angle was calcul-

(CC) 2018 SCS.

ated as 41.75° for optimized structure. In order to compare the theoretical results with the experimental values, the root mean square error (*RMSE*) was used. The calculated *RMSE* for bond lengths and bond angles are 0.026 Å and 2.34°, respectively. These differences could result from the environments in which experimental and theoretical data were obtained. Namely, the theoretical computations were performed in gaseous phase for isolated molecules, whereas the experimental analyses were recorded in the solid phase of the title molecule. The inter-molecular hydrogen bonding interactions in the solid phase (the C7–H7···O1 hydrogen bonds depicted in Fig. S-6) were ignored in the theoretical calculations. Due to the O1–H1···N1 intra-molecular hydrogen bonding interaction, the C2–C1–C7–N1 torsional angle was recorded and calculated as –2.3 and 0.6°, respectively. However, the N2–C8–N1–C7 torsional angles between other groups and pyridine ring (do not exposure any interaction within the theoretical calculations) were measured and computed as 178.0 and 140.4°, respectively.

TABLE III. Some selected molecular structure parameters

Parameter	Bond distance, Å		Parameter	Bond angle, °	
	Experimental	B3LYP		Experimental	B3LYP
C1–C6	1.403 (4)	1.407	C6–C1–C2	118.6 (2)	119.3
C1–C2	1.411 (3)	1.420	C6–C1–C7	119.5 (2)	119.3
C2–O1	1.353 (3)	1.337	O1–C2–C1	121. 2 (2)	122.3
C3–C4	1.373 (4)	1.385	O1–C2–C3	118.8 (2)	118.5
C5–Cl1	1.743 (3)	1.760	C6–C5–Cl1	119.6 (2)	119.9
C7–N1	1.278 (3)	1.285	N1–C7–C1	122.2 (2)	121. 9
C8–N2	1.381 (4)	1.336	N2–C8–C9	117.5 (2)	122.7
C8–N1	1.418 (3)	1.406	N2–C8–N1	118.1 (2)	115.1
C9–C10	1.343 (4)	1.389	C10–C9–C8	123.7 (3)	118.4
C10–C11	1.334 (4)	1.392	C11–C12–N2	119.4 (3)	123.8
C12–N2	1.383 (4)	1.333	C7–N1–C8	121.7 (2)	121.1
C11–C12	1.372 (4)	1.393	C8–N2–C12	119.1 (3)	117.8
Max. Dif.		0.058			5.3
RMSE		0.026			2.34
	Experimental B3LYP				
	Torsion angle, °				
C1–C7–N1–C8	–179.1 (2)	177.7			
O1–C2–C1–C7	1.0 (4)	0			
C7–N1–C8–N2	178.0 (2)	140.4			
N1–C8–C9–C10	–179.6 (3)	–178.8			

HOMO–LUMO analyses and tautomeric stability

The highest occupied molecular orbital (HOMO) represents the outermost orbital filled by electrons and behaves as an electron donor, while the lowest unoccupied molecular orbital (LUMO), considered as the first empty innermost orbital unfilled by electron, behaves as an electron acceptor. In this study, the

(CC) 2018 SCS.

HOMO–1, HOMO, LUMO and LUMO+1 energies and their shapes in the compound are shown in Fig. 2. As seen from Fig. 2, HOMO–1, HOMO and LUMO electrons are localized over almost the whole molecule, whereas LUMO+1 ones are placed on other groups, excepting the 5-chloro-2-hydroxyphenyl ring. The concept of chemical hardness is quite useful in explaining chemical stability. Molecules having a large HOMO–LUMO energy gap will be more stable and less reactive than soft molecules having a small HOMO–LUMO energy gap.[34,35] To investigate the tautomeric stability, optimization calculations at B3LYP/6--311++G(d,p) level were performed for O–H···N in the phenol-imine (OH) and for N–H···O in the keto-amine (NH) forms of the compound. In addition, the total energy, I (ionization potential), A (electron affinity), χ (electronegativity), ζ (softness), ψ (electrophilicity index) and η (chemical hardness)[36] were calculated at the same level and the results are given in Table IV. The total energy of the OH form is lower than that of the NH form, while the chemical hardness of the OH form is greater than that of the NH form, which indicates that the OH form of the compound is more stable than its NH form in the gas phase.[15,37]

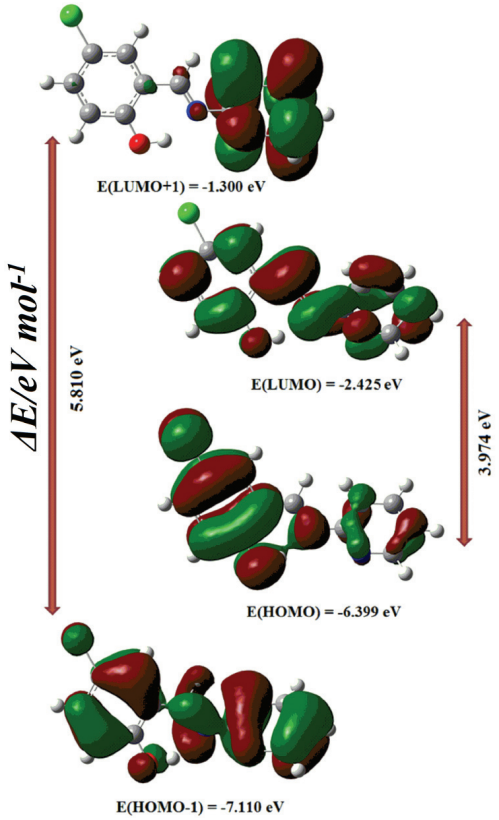

Fig. 2. The molecular orbital surfaces and their energy values of the title compound.

(CC) 2018 SCS.

TABLE IV. The calculated quantum molecular descriptors of the title compound

Parameter	Phenol-imine B3LYP/6-311++G(d,p)	Keto-amine B3LYP/6-311++G(d,p)
E_{total} / Hartree (atomic unit of energy)	–1107.81804145	–1107.81351026
E_{HOMO} / eV	–6.399	–5.885
E_{LUMO} / eV	–2.425	–2.765
E_{HOMO}–E_{LUMO} / eV	3.974	3.120
Ionization potential [$I = -E_{HOMO}$], eV	6.399	5.885
Electron affinity [$A = -E_{LUMO}$], eV	2.425	2.765
Chemical hardness [$\eta = (I - A)/2$], eV	1.987	1.560
Electronegativity [$\chi = -(I + A)/2$], eV	–4.412	–4.325
Softness [$\zeta = 1/2\eta$], eV	0.251	0.320
Electrophilicity index [$\psi = \chi^2/2\eta$], eV	4.898	5.995

The molecular electrostatic potential $V(r)$ is created in the space around a molecule by its nuclei and electrons. It is defined by Eq. (1):

$$V(r) = \sum_{A} \frac{Z_A}{R_A - r} - \int \frac{\rho(r')}{r' - r} dr' \quad (1)$$

in which Z_A is the charge of nucleus A, located at R_A, $\rho(r')$ is the electronic density function of the molecule, and r' is the dummy integration variable.[38] *MEP* is related to the electronic density and is a very useful descriptor in determining sites for electrophilic and nucleophilic reactions as well as hydrogen bonding interactions.[39,40] The *MEP* at the B3LYP/6-311++G(d,p) optimized geometry was calculated.

The red color parts represent the negative electrostatic potential regions or electrophilic reactivity, while blue ones represent the positive ones or nucleophilic reactivity.[41] As could be seen in Fig. 3, a negative region of the compound was observed around the pyridine rings N2 atom. The negative V(r) value is –0.048 a.u. for the N2 atom. A maximum positive region localized on the C7–H7

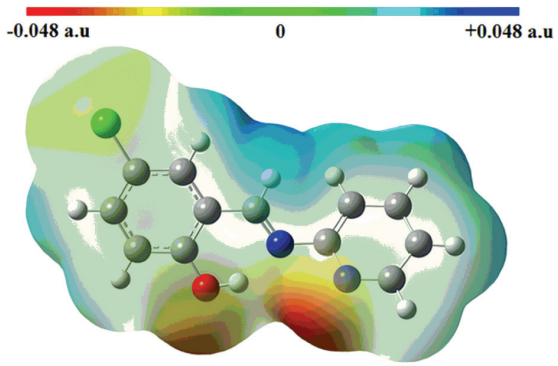

Fig. 3. Molecular electrostatic potential map calculated at the B3LYP/6-311++G(d,p) level.

(CC) 2018 SCS.

bond, indicates a possible site for nucleophilic attack. These values give information about the region from where the compound could have intermolecular interactions. Thus, Fig. 3 confirms the existence of the intermolecular C–H···O hydrogen bond interactions.

Non-linear optical effects

NLO materials have potential applications in optical technology and industrial applications.[42] The NLO values for the compound were calculated at the B3LYP/6-311++G(d,p) level using the Gaussian 09W program package. The equations for calculating the magnitude of total static dipole moment μ_{total}, the mean polarizability $<\alpha>$, the anisotropy of the polarizability $\Delta\alpha$, and the mean first hyperpolarizability (β) using the x, y, z components are defined as:[43,44]

$$\mu = \sqrt{\mu_x^2 + \mu_y^2 + \mu_z^2} \tag{2}$$

$$<\alpha> = \frac{\alpha_{xx} + \alpha_{yy} + \alpha_{zz}}{3} \tag{3}$$

$$\Delta\alpha = \left\{\frac{1}{2}\left[\left(\alpha_{xx} - \alpha_{yy}\right)^2 + \left(\alpha_{xx} - \alpha_{zz}\right)^2 + \left(\alpha_{yy} - \alpha_{zz}\right)^2 + 6\left(\alpha_{xy}^2 + \alpha_{xz}^2 + \alpha_{yz}^2\right)\right]\right\}^{1/2} \tag{4}$$

$$\beta = \sqrt{\left(\beta_{xxx} + \beta_{xyy} + \beta_{xzz}\right)^2 + \left(\beta_{yyy} + \beta_{xxy} + \beta_{yzz}\right)^2 + \left(\beta_{zzz} + \beta_{xxz} + \beta_{yyz}\right)^2} \tag{5}$$

It is well known that higher values of the linear polarizability and the first hyperpolarizability are important key factors for molecules with effective NLO properties. The polarizabilities and first hyperpolarizability are reported in terms of atomic units (a.u.) and the calculated values were converted using 1 a.u = = 0.1482×10^{-24} electrostatic unit (esu) for α and 1 a.u = 8.6393×10^{-33} esu for β. The calculated mean polarizability $<\alpha>$, the anisotropy of the polarizability ($\Delta\alpha$) and the first hyperpolarizability (β) for the studied compound are 28.5354266×10^{-24}, 55.741745×10^{-24} and 77.5621354×10^{-31} esu, respectively (Table V). Urea is one of the essential molecules used for the determination of the NLO properties of molecular systems. Therefore, it is usually used as a reference molecule in NLO studies. The calculated values of urea with the same basis set are 4.9066694×10^{-24} esu for $<\alpha>$ and 7.8781964×10^{-31} esu for β. According to these results, the mean polarizability and first hyperpolarizability of the studied compound are approximately 5.81 and 9.845 times greater than those of urea, which implies that the title compound is a good candidate material for NLO applications.

(CC) 2018 SCS.

TABLE V. The computed dipole moments, polarizability and first hyperpolarizability values of the title compound

Parameter	a.u.	esu×10^{24}	Parameter	a.u.	esu×10^{31}
α_{xx}	311.1872364	46.1179484	β_{xxx}	–722.1630436	62.3898318
α_{xy}	4.4930217	0.6658658	β_{xxy}	–285.766783	24.6882496
α_{xz}	–4.7262655	0.7004325	β_{xyy}	–72.2753195	6.2440816
α_{yy}	167.2074794	24.7801484	β_{yyy}	–71.7018625	6.1945390
α_{yz}	5.6208234	0.8330060	β_{xxz}	84.4473294	7.2956581
α_{zz}	99.2454993	14.7081829	β_{yyz}	26.8613951	2.3206365
α_{total}	192.5467383	28.5354266	β_{xzz}	–15.1811256	1.3115429
$\Delta\alpha$	376.12331457	55.741745	β_{yzz}	–15.7126661	1.3574643
μ_x	–2.1621		β_{zzz}	–5.1689098	0.4465576
μ_y	–2.7821		β	897.7826375	77.5621354
μ_z	–0.8375				
μ_{total}	3.6216				

FTIR, ^{1}H-NMR, ^{13}C-NMR and UV spectroscopy

The vibration bands with the wave numbers 3433 cm^{-1} (broad strong, O–H); 3107–3046 cm^{-1} (weak, Ar-H); 1560 cm^{-1} (strong, C=C); 1478 cm^{-1} (strong, C–N) and 1356 cm^{-1} (strong, Ar–O) were observed for the compound (Fig. S-2). The C=N bond was observed at 1616 cm^{-1} for the compound. The stretching frequency observed at 2852–2750 cm^{-1} in the spectrum of the compound showed the presence of O–H···N intramolecular hydrogen bonds.[45,46] The C=N bond, which is partially accountable for the existence of the phenol-imine form, can also be inferred from the IR spectrum of the compound. A compound with strong band at 1274 cm^{-1} possessed high percentages of the phenol-imine tautomer due to stabilization of the phenolic C–O bond.[47]

The ^{1}H-NMR data for the compound show that the tautomeric equilibrium favors the phenol-imine form in DMSO (Fig. S-3). The OH proton was observed as a singlet at 12.49 ppm for the compound. The azomethine proton was observed as a singlet at 8.94 ppm for the compound. The phenyl protons of the compound resonated as multiplet between 8.60–6.96 ppm.

According to the proton de-coupled ^{13}C-NMR spectra, the compound has 12 signals in deutero-DMSO (Fig. S-4). The azomethine carbon (Ar**C**H=N–) is observed at δ = 164.15 ppm for the Schiff base. In the investigated compound, the aromatic-C chemical shifts (δ / ppm) are 164.15, 158.80, 148.73, 144.89, 144.24, 133.60, 130.99, 128.17, 124.64, 123.05, 121.20 and 119.61.

The UV–Vis spectra of the compound were studied in DMSO (Fig. S-5). Schiff bases exhibited absorptions in the range greater than 400 nm in polar and nonpolar solvents. The UV–Vis spectrum of *ortho* hydroxylated Schiff-bases that exist mainly as the phenol-imine structure is indicated by the presence of a band at < 400 nm, while compounds existing either as keto-amine or as mixture of

(CC) 2018 SCS.

phenol-imine/keto-amine forms show a new band, especially in polar and non-polar solvents in both acidic and basic media, at >400 nm. [45–47] The title compound showed no absorption above 400 nm in DMSO, indicating that the compound exists in the phenol-imine form in DMSO. In conclusion, UV-Vis, ^{1}H-NMR and ^{13}C-NMR results showed that the compound existed in the phenol-imine form in DMSO.

*Minimum inhibitory concentration (*MIC*)*

The *MIC* was evaluated by the broth micro dilution test. The *MIC* values were read as the lowest concentration of the drug in the series that prevents the development of visible growth of the test organism. The data reported in Table VI are the average from three experiments.

The antimicrobial activity spectrum of the Schiff base varied in the concentration range 32–128 μg mL^{-1}. It could be observed from Table VI that the Schiff base exhibited a high antifungal effect on *C. albicans* and *C. tropicalis*, while the compound had a low effect on the bacteria. However, the compound had stronger antibacterial effect against *S. aureus*, *E. faecalis*, *B. cereus* NRRL B-3711, *E. coli* ATCC 25922, *E. coli* ATCC 35218, *P. aeruginosa* and *P. hauseri* compared to *B. subtilis*. Furthermore, this compound showed similar activity against the tested microorganisms, despite the fact that the cell wall in Gram-positive bacteria have a single layer, whereas the Gram-negative cell wall is a multi-layered structure, and the yeast cell wall is quite complex. The antifungal activity of the compound was found to be dose dependent with MIC of 32 μg mL^{-1}.

TABLE VI. *MIC* value (μg mL^{-1}) of the compound

Microorganism	Compound	Antibiotic	
	Schiff base	Ampicillin	Fluconazole
S. aureus ATCC 25923	64	1	–
E. faecalis ATCC 29212	64	2	–
B. cereus NRRL B-3711	64	2	–
B. subtilis ATCC 6633	128	1	–
E. coli ATCC 25922	64	16	–
E. coli ATCC 35218	64	32	–
P. aeruginosa ATCC 27853	64	2	–
P. hauseri ATCC 13315	64	2	–
C. albicans ATCC 60193	32	–	16
C. tropicalis ATCC 13803	32	–	32

DNA-binding

The potential binding ability of the compound to CT-DNA was characterized by UV spectroscopy. The absorption spectra of the ligand in the absence and presence of CT-DNA at different concentrations are given in Fig. 4. Absorption spectroscopy is one of the most used methods for investigating the effects of any

(CC) 2018 SCS.

material on DNA. If it has an intercalation effect against DNA, generally a hypochromic effect is observed. However, if the interaction of a material with DNA is electrostatic or partially intercalative, a hyperchromic effect is observed.[4,5,15] Moreover, a red shift of the absorption maximum indicates that the difference between HOMO and LUMO energy levels decreases, and that the complex interacts with DNA.[4] The absorption spectra of the Schiff base in the absence and the presence of CT-DNA are shown in Fig. 4. In the UV region, two intense bands absorbed at 269 and 386 nm for the ligand. In the presence of CT-DNA, an increase in the peak intensities was observed in the absorption spectra of Schiff base. In addition to the increase in intensity, a small red shift (bathochromism; 1–7 nm) was also observed in the spectra for Schiff base. The absorption intensity of the band at 269 nm of the ligand increased (hyperchromism) evidently after the addition of CT-DNA (0, 0.5, 1, 2, 3, 4, 5, 6, 7 and 8 μL), which indicated the interactions between DNA and the Schiff base (Fig. 4). The extent of red shift and hyperchromism are commonly found to correlate with the electrostatic binding strength. Consequently, the observation of hyperchromic effect in the absorption spectra implies that the ligand established an electrostatic bond with DNA. In the electrostatic binding, DNA breaks phenol protons from the more acidic Schiff base. As a result, the negative charge distribution is changed in the DNA chain, thereby, leading to disruption of the DNA molecules.

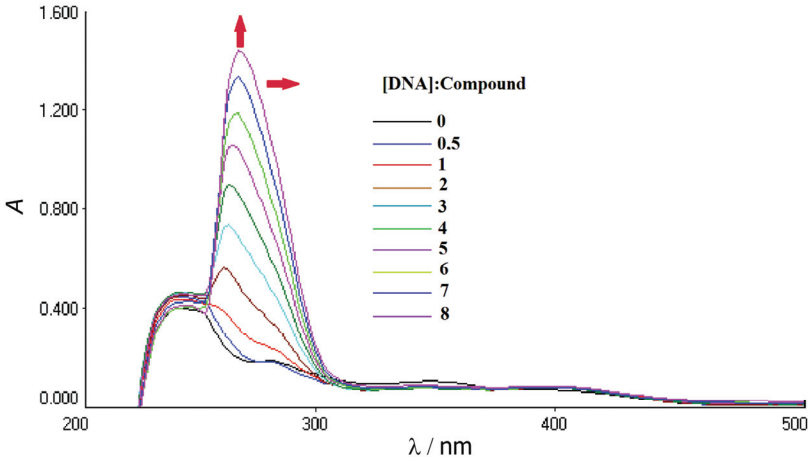

Fig. 4. Absorption spectra of the compound in the absence and presence of increasing amounts of CT-DNA at room temperature in Tris–HCl/NaCl buffer (pH 7.2).

Colorimetric anion-sensing

In order to investigate whether the Schiff base could be used for visual confirmation of anions in a sample, real color photographs of the corresponding DMSO solutions of the compound with F^-, Br^-, I^-, CN^-, SCN^-, ClO_4^-, HSO_4^-,

(CC) 2018 SCS.

N_3^-, AcO^-, $H_2PO_4^-$ and OH^- as tetrabutylammonium salts were taken and are shown in Fig. 5. After addition of the anions to the Schiff base in DMSO, the color of the solution changed from colorless to yellow and orange with F^-, AcO^-, OH^- and CN^- with fast response time (< 1 s), indicating that receptors in the title compound could serve as a "naked-eye" indicator for F^-, AcO^-, OH^- and CN^-.

The more acidic phenol proton would deprotonate upon exposure to more basic OH^-, F^- and AcO^- and therefore, intramolecular proton transfer occurs into the keto-amine form. In contrast, CN^- has much weaker hydrogen bonding ability in comparison with OH^-, F^- and AcO^- with a stronger nucleophilicity toward the imine group, which results in the addition reaction of CN^- to the carbon atom of an electron deficient imine group and, subsequently, fast proton transfer of the phenol hydrogen to the neighboring nitrogen anion through an intramolecular hydrogen bond.[15] The formation of the keto-amine form of the compound leads to higher wavelength absorptions.

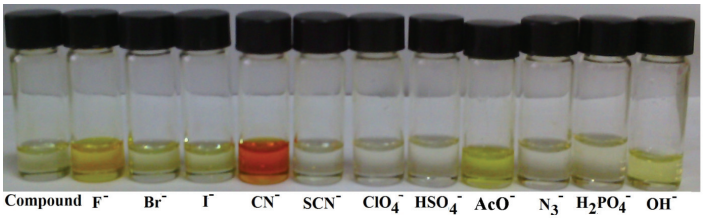

Fig. 5. The color changes of the compound (1 equiv.) upon addition of various anions (1 equiv.) of the compound.

CONCLUSIONS

In this study, (*E*)-4-chloro-2-[(pyridin-2-ylimino)methyl]phenol is reported. The molecular structure of the compound was confirmed by X-ray crystallographic, elemental analysis, UV–Vis, NMR and FTIR studies. Theoretical calculations were employed to determine the molecular structure, spectroscopic values, and HOMO and LUMO levels of the title compound. The theoretical calculations were found to be in good agreement with the experimental data. The theoretical evaluation of the NLO properties showed that the title compound has larger polarizability and hyperpolarizability values than urea, which denotes its use in potential NLO applications. The ligand was found to act as anti-microbial, DNA--binding and anion sensor agent.

Acknowledgement. The authors are grateful to the Scientific and Technical Research Council of Turkey (TÜBİTAK) for the financial support of this work, Grant No. TÜBİTAK 115F253.

SUPPLEMENTARY MATERIAL

Further information may be obtained from Cambridge Crystallographic Data Centre (CCDC), 12 Union Road, Cambridge CB21EZ, UK, by quoting the depository number CCDC 1564849, e-mail: deposit@ccdc.cam. ac.uk.

(CC) 2018 SCS.

Theoretical and spectral data of the title compound are available electronically at the pages of journal website: http://www.shd.org.rs/JSCS/, or from the corresponding author on request.

ИЗВОД

DFT ИЗРАЧУНАВАЊЕ, БИОЛОШКА АКТИВНОСТ, ПРОУЧАВАЊЕ ДЕТЕКЦИЈЕ АНЈОНА И КРИСТАЛНА СТРУКТУРА (*E*)-4-ХЛОРО-2-[(ПИРИДИН-2-ИЛИМИНО)-МЕТИЛ]ФЕНОЛА

NURAY YILDIRIM[1], NESLİHAN DEMİR[2], GÖKHAN ALPASLAN[3], BAHADIR BOYACIOĞLU[4], MUSTAFA YILDIZ[5] и HÜSEYİN ÜNVER[6]

[1]Health Services Vocational School, Çanakkale Onsekiz Mart University, TR-17100 Çanakkale, Turkey, [2]Department of Biology, Faculty of Arts and Sciences, Çanakkale Onsekiz Mart University, TR-17100 Çanakkale, Turkey, [3]Department of Medical Services and Techniques, Vocational School of Health Services, Giresun University, TR-28200 Giresun, Turkey, [4]Vocational School of Health Services, Ankara University, TR-06290 Keçioren-Ankara, Turkey, [5]Department of Chemistry, Faculty of Arts and Sciences, Çanakkale Onsekiz Mart University, TR-17100 Çanakkale, Turkey and [6]Department of Physics, Faculty of Science, Ankara University, 06100 Beşevler-Ankara, Turkey

(*E*)-4-Хлоро-2-[(пиридин-2-илимино)метил]фенол је синтетисан реакцијом 2-аминопиридина са 5-хлоросалицилалдхидом. Структура једињења је истраживана са FTIR, UV–Vis, ^{1}H-NMR, ^{13}C-NMR и дифракцијом X-зрака (XRD). Карактеризација једињења је такође урађена коришћењем теоријских квантномеханичких израчунавања и експерименталних спектроскопских метода. Молекулска структура једињења је потврђена XRD, NMR, FTIR и UV–Vis подацима који су били у доброј сагласности са структуром претсказаном теоријским израчунавањем, коришћењем методе функционала густине (DFT). Надаље, истраживана је антимикробна активност једињења на културама бактерија и квасца тестом разблаживања хранљивог медијума. UV–Vis спектроскопске студије интеракција између Шифових (Schiff) база и DNK говеђег тимуса (CT-DNA), показала су да једињење интерагује са CT-DNA путем електростатског везивања. Колориметријски одговор рецептора овог једињења истражен је пре и након додатка еквивалентне количине разних анјона како би се проценили особине препознавања анјона.

(Примљено 2. октобра, ревидирано 28. новембра, прихваћено 25. децембра 2017)

REFERENCES

1. P. Li, M. J. Niu, M. Hong, S. Cheng, J. M. Dou, *J. Inorg. Biochem*. **137** (2014) 101
2. M. J. Niu, D. W. Sun, H. H. Li, Z. Q. Cao, S. N. Wang, J. M. Dou, *J. Coord. Chem*. **67** (2014) 81
3. J. Haribabu, K. Jeyalakshmi, Y. Arun, N. S. P. Bhuvanesh, P. T. Perumal, R. Karvembu, *RSC Adv.* **5** (2015) 46031
4. F. Arjmand, M. Aziz, *Eur. J. Med. Chem*. **44** (2009) 834
5. P. Li, M. F. Niu, M. J. Niu, M. Hong, *Z. Anorg. Allg. Chem*. **640** (2014) 2238
6. S. A. Khan, A. A. Siddiqui, S. Bhatt, *Asian J. Chem*. **14** (2002) 1117
7. S. N. Pandeya, D. Sriram, G. Nath, E. DeClercq, *Eur. J. Pharm. Sci*. **9** (1999) 25
8. P. G. More, R. B. Bhalvankar, S. C. Pattar, *J. Indian Chem. Soc*. **78** (2001) 474
9. N. Solak, S. Rollas, *ARKIVOC* **2006** (2006) (xii) 173
10. P. K. Panchal, H. M. Parekh, P. B. Pansuriya, M. N. Patel, *J. Enzyme Inhib. Med. Chem*. **21** (2006) 203
11. N. K. Chaudhary, P. Mishra, *Bioinorg. Chem. Appl*. **2017** (2017) 1
12. D. Chaturvedi, M. Kamboj, *Chem. Sci. J*. **7** (2016) 1
13. A. Koll, M. Rospenk, E. Jagodzinska, T. Dziembowska, *J. Mol. Struct*. **552** (2000) 193

(CC) 2018 SCS.

14. V. Razakantoanina, N. K. P. Phung, G. Jaureguiberry, *Parasitol. Res*. **86** (2000) 665
15. M. Yıldız, Ö. Karpuz, C. T. Zeyrek, B. Boyacıoğlu, H. Dal, N. Demir, N. Yıldırım, H. Ünver, *J. Mol. Struct*. **1094** (2015) 148
16. B. Barare, M. Yıldız, G. Alpaslan, N. Dilek, H. Ünver, S. Tadesse, K. Aslan, *Sens. Actuators, B* **215** (2015) 52
17. M. Yıldız, E. Tan, N. Demir, N. Yıldırım, H. Ünver, A. Kiraz, B. Mestav, *Russ. J. Gen. Chem*. **85** (2015) 2149
18. Y. P. Li, H. Lin, Z. S. Cai, H. K. Lin, *Mini-Rev. Org. Chem*. **8** (2011) 25
19. D. Sharma, A. R. Mistry, R. K. Bera, S. K. Sahoo, *Supramol. Chem*. **25** (2013) 212
20. Bruker, APEX2 and SAINT, Bruker AXS Inc., Madison, WI, 2007
21. Bruker, SADABS, Bruker AXS Inc., Madison, WI, 2005
22. G. M. Sheldrick, *Acta Crystallogr*., Sect. *A* **64** (2008) 112
23. C. F. Macrae, P. R. Edgington, P. McCabe, E. Pidcock, G. P. Shields, R. Taylor, M. Towler, J. Van de Streek. *J. Appl. Crystallogr*. **39** (2006) 453
24. L. J. Farrugia, *J. Appl. Crystallogr*. **45** (2012) 849
25. R. Dennington II, T. Keith, J. Millam, *GaussView, Version 5*, Semichem Inc., Shawnee Mission, KS, 2009
26. *Gaussian 09, Revision D.01*, Gaussian Inc., Wallingford, CT, 2009
27. A. D. Becke, *J. Chem. Phys*. **98** (1993) 5648
28. C. Peng, P. Y. Ayala, H. B. Schlegel, M. J. Frisch, *J. Comput. Chem*. **17** (1996) 49
29. CLSI, *Methods for Dilution Antimicrobial Susceptibility Tests for Bacteria That Grow Aerobically; Approved Standard*, 10th ed., CLSI document M07-A10, Clinical and Laboratory Standards Institute, Wayne, PA, 2015
30. J. Marmur, *J. Mol. Biol*. **3** (1961) 208
31. H. Ünver, M. Yıldız, A. Kiraz, N. O. Iskeleli, A. Erdönmez, B. Dülger, T. N. Durlu, *J. Chem. Crystallogr*. **36** (2006) 229
32. H. Tanak. *J. Phys. Chem*. *A* **115** (2011) 13865
33. G. Alpaslan, M. Macit. *Spectrochim. Acta,Part A* **121** (2014) 372
34. K. Fukui, *Science* **218** (1982) 747
35. H. Gökce, S. Bahçeli, *Spectrochim. Acta, Part A* **79** (2011) 1783
36. A. Soltani, F. Ghari, A. D. Khalaji, E. T. Lemeski, K. Fejfarova, M. Dusek, M. Shikhi, *Spectrochim. Acta, A* **139** (2015) 271
37. Z. S. Marković, N. T. Manojlović, S. R. Jeremić, M. Živić, *Hem. Ind.* **67** (2013) 77
38. P. Politzer, P. Lane, *Struct. Chem*. **1** (1990) 159
39. E. Scrocco, J. Tomasi, in *Topics in Current Chemistry, New Concepts II*, No. 42. Springer-Verlag, Berlin, 1973, pp. 95–170
40. F. J. Luque, J. M. Lopez, M. Orozco, *Theor. Chem. Acc*. **103** (2000) 343
41. E. H. Avdović, D. Milenković, J. M. Dimitrić-Marković, N. Vuković, S. R. Trifunović, Z. Marković, *J. Mol. Struct*. **1147** (2017) 69
42. D. R. Kanis, M. A. Ratner, T. J. Marks, *Chem. Rev*. **94** (1994) 195
43. R. Zhang, B. Du, G. Sun, Y. Sun, *Spectrochim. Acta, A* **75** (2010) 1115
44. A. Alparone, *Chem. Phys*. **410** (2013) 90
45. M. Yildiz, Z. Kilic, T. Hokelek, *J. Mol. Struct*. **441** (1998) 1
46. H. Nazir, M. Yildiz, H. Yilmaz, M. N. Tahir, D. Ulku, *J. Mol. Struct*. **52** (2000) 241
47. G. Y. Yeap, S. T. Ha, N. Ishizawa, K. Suda, P. L Boey, W. A. K. Mahmood, *J. Mol. Struct*. **658** (2003) 87.

(CC) 2018 SCS.